Tapping-Mode Atomic Force Microscopy Produces Faithful High-Resolution Images of Protein Surfaces

Clemens Möller,*# Mike Allen,§ Virgil Elings,§ Andreas Engel,* and Daniel J. Müller*

*M. E. Müller Institute for Structural Biology, Biozentrum, CH-4056 Basel, Switzerland; #Forschungszentrum Jülich, IBI-2: Structural Biology, D-52425 Jülich, Germany; and §Digital Instruments, Santa Barbara, California 93117 USA

ABSTRACT Compared to contact-mode atomic force microscopy (CMAFM), tapping-mode atomic force microscopy (TMAFM) has the advantage of allowing imaging surfaces of macromolecules, even when they are only weakly attached to the support. In this study, TMAFM is applied to two different regular protein layers whose structures are known to great detail, the purple membrane from *Halobacterium salinarum* and the hexagonally packed intermediate (HPI) layer from *Deinococcus radiodurans*, to assess the faithfulness of high-resolution TMAFM images. Topographs exhibited a lateral resolution between 1.1 and 1.5 nm and a vertical resolution of ~0.1 nm. For all protein surfaces, TMAFM and CMAFM topographs were in excellent agreement. TMAFM was capable of imaging the fragile polypeptide loop connecting the transmembrane α-helices E and F of bacteriorhodopsin in its native extended conformation. The standard deviation (SD) of averages calculated from TMAFM topographs exhibited an enhanced minimum (between 0.1 and 0.9 nm) that can be assigned to the higher noise of the raw data. However, the SD difference, indicating the flexibility of protein subunits, exhibited an excellent agreement between the two imaging modes. This demonstrates that the recently invented imaging-mode TMAFM has the ability to faithfully record high-resolution images and has sufficient sensitivity to contour individual peptide loops without detectable deformations.

INTRODUCTION

The atomic force microscope (AFM) (Binnig et al., 1986) has several features that are attractive to the biologist. Most importantly, biological structures can be observed in their native state in buffer solution. The high signal-to-noise (S/N) ratio of the AFM allows imaging of whole cells as well as their components, such as proteins or nucleic acids (Drake et al., 1989). The AFM can further be used to capture dynamic aspects of individual biological molecules (Bezanilla et al., 1994; Kasas et al., 1997; Müller et al., 1997b; Shlyakhtenko et al., 1998; Engel et al., 1999; Müller and Engel, 1999) and their interactions with the environment (Butt, 1992; Radmacher et al., 1994a,b), providing new insights into how macromolecules may work on the nanometer scale. Recent and ongoing developments of new scanning probe microscopes (Wiesendanger, 1994; Colton et al., 1998; Hörber et al., 1998) aim at imaging the high-resolution topography of a biological molecule while simultaneously revealing intrinsic properties such as flexibility (Müller et al., 1998) and surface potentials (Müller and Engel, 1997; Czajkowsky et al., 1998a).

Until now, high-resolution images of native proteins were exclusively acquired with the AFM in the contact mode (Hoh et al., 1993; Karrasch et al., 1993, 1994; Yang et al., 1993, 1994; Schabert et al., 1995). Continuous improvements of the preparation techniques (Karrasch et al., 1993; Müller et al., 1997a; Czajkowsky et al., 1998b; Wagner, 1998; Scheuring et al., 1999) and imaging conditions (Müller et al., 1999a) made it possible to contour native proteins at a lateral resolution of ~0.5 nm and a vertical resolution of ~0.1 nm (Müller and Engel, 1999; Müller et al., 1999b). However, contact mode imaging turned out to be less suitable for weakly immobilized structures, as single macromolecules are often pushed away by the AFM stylus during raster scanning of the surface (Karrasch et al., 1993). To overcome this disadvantage, tapping-mode atomic force microscopy (TMAFM) has been developed (Zhong et al., 1993; Hansma et al., 1994; Putman et al., 1994). In tapping mode, the stylus oscillates, touching the sample only at the end of its downward movement, which reduces the contact time and the friction forces compared to contact-mode AFM (CMAFM). Thus a variety of macromolecules have been observed (Bezanilla et al., 1994; Radmacher et al., 1994b; Fritz et al., 1995a,b; Martin et al., 1995; Dunlap et al., 1997; Kasas et al., 1997; Lyubchenko and Shlyakhtenko, 1997; Shlyakhtenko et al., 1998) that could not be imaged with CMAFM. Despite this advantage, TMAFM lacked the resolution achieved by CMAFM.

Here we demonstrate that by optimizing imaging parameters TMAFM produces faithful high-resolution images of native protein surfaces and, in theory, could be applied to a wide range of biological systems. We have selected the hexagonally packed intermediate (HPI) layer of *Deinococcus radiodurans* (Baumeister et al., 1982) and the purple membrane of *Halobacterium salinarum* (Oesterhelt and Stoeckenius, 1973; Oesterhelt, 1998) as test specimens, because their three-dimensional structures are known (Baumeister et al., 1986; Jakubowski et al., 1988; Grigorieff

Received for publication 8 February 1999 and in final form 30 April 1999.

Address reprint requests to Dr. Daniel J. Müller or Dr. Andreas Engel, M. E. Müller Institute for Structural Biology, Biozentrum, University of Basel, Klingelbergstrasse 70, CH-4056 Basel, Switzerland. Tel.: 0041-61-267-22-55; Fax: 0041-61-267-21-09; E-mail: muellerda@ubaclu.unibas.ch.

C. Möller and M. Allen contributed equally to this work.

0006-3495/99/08/1150/09 $2.00

et al., 1996; Kimura et al., 1997) and their surfaces have been investigated by CMAFM (Karrasch et al., 1994; Müller et al., 1995a, 1996a,b, 1999b). Bacteriorhodopsin, the major constituent of the purple membrane, exhibits a cytoplasmic peptide loop connecting transmembrane α-helices E and F that can undergo a force-induced conformational change (Müller et al., 1995a, 1999b). This E-F loop remains in its extended state as long as the force applied to the AFM stylus is $\leq$100 pN, being reversibly bent toward the protein surface at higher forces. Hence, purple membrane is most suitable for testing the sensitivity of TMAFM. Standard deviation maps calculated from aligned high-resolution topographs of individual protein complexes allow their variable surface regions to be located (Müller et al., 1998). We have compared these regions with those revealed from high-resolution contact-mode topographs and demonstrate here that TMAFM produces faithful images of individual polypeptide domains without detectable deformation.

MATERIALS AND METHODS

Atomic force microscopy

Instrumental set-up

A commercial TMAFM (Nanoscope IIIa; Digital Instruments, Santa Barbara, CA) equipped with either a 12-μm scanner (E-scanner) or a 120-μm scanner (J-scanner) and a tapping-mode liquid cell without an O-ring seal was employed. Before use the liquid cell was cleaned with normal dish cleaner, gently rinsed with ultrapure water ($\sim$18 MΩ/cm; Branstead, Boston, MA), cleaned with ethanol, and finally rinsed with ultrapure water. Muscovite Mica (Mica New York Corp., New York, NY), punched to a diameter of $\sim$5 mm, or a small square ($\sim 5 \times 5$ mm) of highly oriented pyrolitic graphite (HOPG) (Advanced Ceramics, Cleveland, OH) was glued with water-insoluble epoxy glue (Araldit; Novartis AG, Basel, Switzerland) to a Teflon disc. Its diameter of 25 mm was slightly larger than the diameter of the supporting steel disc. The steel disc was required to magnetically mount the sample on the piezoelectric scanner. For high-resolution imaging the TMAFM was placed on a vibration-isolated stone plate.

Imaging using tapping-mode atomic force microscopy

High-resolution imaging using the TMAFM required its operation at drive frequencies close to 8.7 ± 0.5 kHz. This resonance peak of the TMAFM liquid cell immersed in buffer solution (fluid drive spectrum; Schäffer et al., 1996) was particularly suited to operation of the TMAFM because it was close to and within the range of the natural resonance frequency of the cantilever immersed in aqueous solution (8.9 ± 1 kHz), as determined by the thermal noise spectrum (Butt and Jaschke, 1995; Salapaka et al., 1997). The resonance frequencies of the cantilevers mounted in the fluid cell had a full width at half-maximum of $\leq$0.5 kHz. Activating the cantilever within this frequency range ensured that the cantilever response was optimized (Schäffer et al., 1996). To achieve an efficient coupling between the drive voltage and cantilever amplitude response, the cantilever was brought to the sample within a distance of 8 μm. The 120-μm-long V-shaped cantilevers purchased from Olympus Ltd. (Tokyo, Japan) had a force constant of $k = 0.1$ N/m and oxide sharpened Si_3N_4 tips.

Before engaging, scan size and offset of the microscope were set to 0 to minimize sample deformation and contamination of the stylus. To engage the AFM stylus, the piezo drive amplitude was set to 100 mV, resulting in a $\sim$0.5-V amplitude (corresponding to $\sim$16 nm with $\sim$4 nm/125 mV) of the cantilever. Before the sample was scanned, the setpoint was adjusted to minimal forces. The amplitude signal was used to activate the feedback loop. Imaging at low magnification (frame size $>$ 1 μm) was performed, acquiring the height and amplitude signal simultaneously. Both the noise of the topograph and the amplitude signals were minimized by optimizing gains and scan speed. As a general rule, gains and scan speed were about a factor of 4 smaller than the typical values used in CMAFM. At high magnifications the topography was simultaneously recorded in the trace and the retrace directions to observe scan artifacts. The raw data presented are height images recorded in the tapping mode. The scan speed was roughly linear to the scan size, 1–2 lines/s for lower magnifications and 2–4 lines/s for higher magnifications (frame size $<$ 1 μm). High resolution was achieved by using drive amplitudes between 25 and 250 mV, corresponding to 1–8 nm of amplitude. Imaging at high resolution required compensation for thermal drift. Therefore, the setpoint was corrected manually in steps of 0.001 V. Typical values for high-resolution imaging were between 0.03 and 0.3 V, depending on the drive amplitude. The difference between the setpoint of jump in and the setpoint adjusted to achieve high-resolution topographs was $\sim$0.02 V, corresponding to a damping of $\sim$1 nm of the free amplitude. Interestingly, the best topographic contrast was obtained when the ratio of drive amplitude and setpoint was close to 1.

Imaging using contact-mode atomic force microscopy

High-resolution CMAFM topographs were obtained using the microscope setup, sample preparation, and cantilevers as described in the TMAFM section. To reveal subnanometer resolution, the electrolyte was adjusted to control the tip-sample interactions (Müller et al., 1999a). Imaging at low magnification (scan size $>$ 500 nm) was performed in the error signal mode. Acquisition of the deflection and height signals was simultaneous (Putman et al., 1992). The deflection signal was minimized by optimizing integral and proportional gains and scan speed. At high magnification (scan size $<$ 200 nm) topographs were scanned simultaneously in the trace and retrace directions. The scan speed was roughly linear to the scan size, 4–8 lines/s for lower magnifications (512 pixels/line and frame size 1–25 μm) and 8–16 lines/s for higher magnifications (frame size $<$ 200 nm). All CMAFM topographs were recorded at applied forces of $\leq$100 pN, which was corrected manually to compensate for thermal drift.

Biological samples

The HPI layer from *Deinococcus radiodurans*, a kind gift of Dr. W. Baumeister, was extracted from whole cells (strain SARK) with lithium dodecyl sulfate and purified on a Percoll density gradient (Baumeister et al., 1982). A stock solution (1 mg/ml protein) was stored in ultrapure water at 4°C.

Purple membranes of *Halobacterium salinarum* strain ET1001, a kind gift of Dr. G. Büldt, were isolated as described by Oesterhelt and Stoeckenius (1974). The membranes were frozen and stored at $-$70°C. After thawing, stock solutions (10 mg protein/ml) were kept in ultrapure water at 4°C.

Sample preparation

We found that TMAFM was extremely sensitive to contamination of sample and tip. To minimize contamination of surfaces, mica was cleaved immediately before use, and buffers were made with ultrapure water. The latter is superior over conventional bidistilled water in that it contains fewer hydrocarbons and fewer macroscopic contaminants, all of which can distort the imaging process. Chemicals were grade p.a. and purchased from Sigma Chemie AG (Buchs, Switzerland). The buffers used were Tris-(hydroxymethyl)-aminomethane (from pH 10.2 to 7.2). The biological samples were routinely checked before use in the AFM by conventional negative stain electron microscopy (Bremer et al., 1992).

The samples were diluted to a concentration of 5–10 μg/ml in buffer solution (pH 8.2, 20 mM Tris-HCl, 300 mM KCl) before adsorption to

freshly cleaved mica. After an adsorption time of 10–60 min at room temperature, the samples were gently washed with the respective imaging buffer (see figure legends) to remove weakly attached membranes (Müller et al., 1997a). This allowed imaging at low electrolyte concentrations, where samples adsorb sparsely to mica.

Image processing

Topographs (512 × 512 pixels) of the protein layers were selected by the crystal order and by comparison of the height profiles acquired in the trace and the retrace directions. For image processing, the raw data were transferred to a Digital Equipment α workstation and analyzed with the SEMPER image processing system (Saxton et al., 1979). For correlation averaging, a well-preserved unit cell was selected from the raw data and cross-correlated with the topograph (Saxton and Baumeister, 1982). The unit cells were then extracted according to the correlation peak coordinates and averaged. Simultaneously, the standard deviation was calculated for each pixel of the unit cell (Schabert and Engel, 1994). The resulting correlation average was used as a reference for refinement cycles. Correlation-averaged unit cells and their standard deviations were finally symmetrized.

RESULTS

Reproducible observation of protein subunits

The HPI layer, a bacterial surface layer, is composed of the major cell envelope protein of the radiotolerant eubacteria *D. radiodurans* (Baumeister et al., 1982). The HPI layer has been characterized biochemically (Baumeister et al., 1982), and structurally by electron microscopy (Baumeister et al., 1986), by atomic force microscopy (Karrasch et al., 1994; Müller et al., 1996a), and by scanning tunneling microscopy (Guckenberger et al., 1989; Wang et al., 1990; Amrein et al., 1991; Stemmer et al., 1991). Assembled from a single protein (M_r 107,028; Peters et al., 1987) that forms hexamers of M_r 655,000 (Engel et al., 1982), the HPI layer is a hexagonal lattice with a unit cell size of 18 nm. A three-dimensional model has been derived from the electron microscopy data (Baumeister et al., 1986), which shows that each hexagonal unit is composed of a massive core enclosing a pore. The subunits have spoke-like protrusions that emanate from the core and provide connections to adjacent units. This arrangement exhibits relatively large openings around the sixfold axes.

HPI layers adsorbed onto freshly cleaved HOPG were imaged with TMAFM in buffer solution. Topographs were stable through multiple scans (Fig. 1 *A–C*) and clearly represented the structural features of the hexagonal units that had previously been observed by 3-D electron microscopy and by CMAFM (Karrasch et al., 1994). Occasionally, single protomers were missing from the hexameric cores, a feature that has often been observed by CMAFM (Karrasch et al., 1993; Müller et al., 1996a, 1998). Submolecular

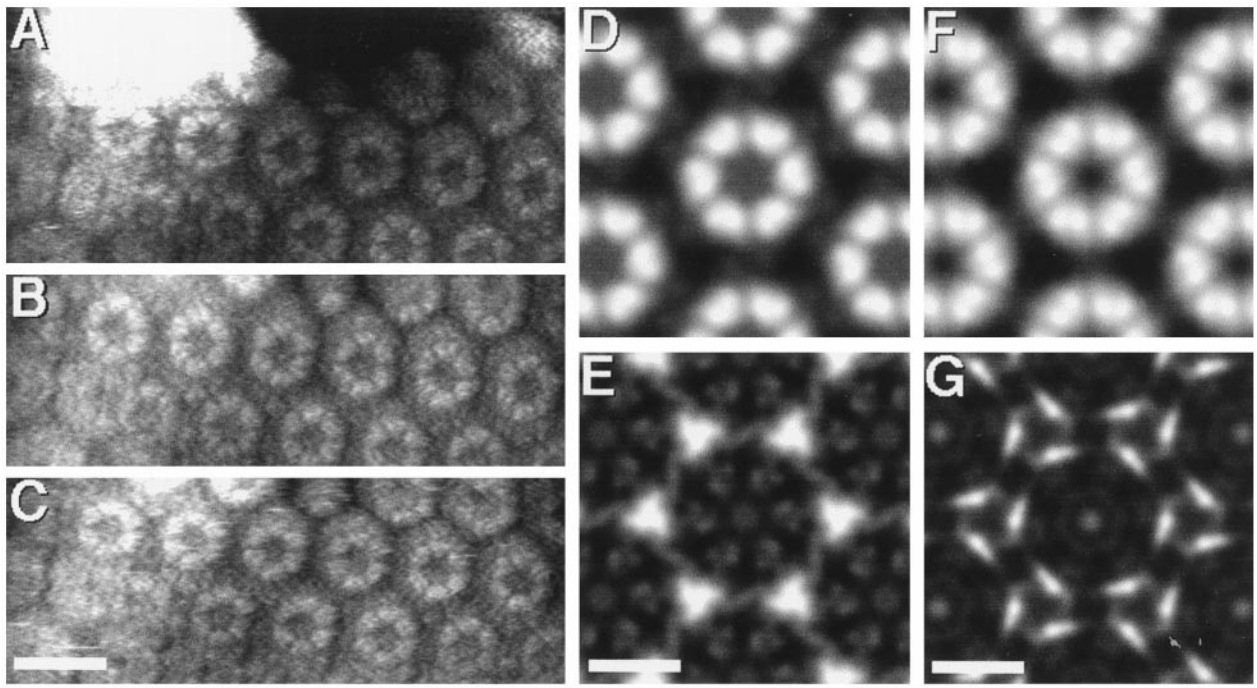

FIGURE 1 Repeated imaging of the outer surface of the HPI layer by TMAFM. (*A*) Raw data obtained in 200 mM KCl, pH 7.8, 20 mM Tris-HCl. (*B* and *C*) Same surface area imaged after 8 and 16 min, respectively. (*D*) Sixfold symmetrized correlation average from 97 unit cells (10.8% root mean square (RMS) deviation from sixfold symmetry). (*E*) Sixfold symmetrized standard deviation map. (*F*) Averaged topograph of the outer HPI layer surface, recorded by CMAFM. The correlation average was sixfold symmetrized ($n = 79$; 2.8% RMS deviation from sixfold symmetry; Müller et al., 1998). (*G*) Sixfold symmetrized standard deviation map of *F*. Full gray-level ranges: 4 nm (*A–C*) and 3 nm (*D* and *F*). Minima and maxima of the standard deviation were 0.62 nm and 0.95 nm for *E* and 0.11 nm and 0.34 nm for *G*. Scale bars: 20 nm (*A–C*) and 10 nm (*E* and *G*). TMAFM imaging conditions: HPI layer adsorbed onto HOPG, original scan size 185 nm, scan frequency 3.8 Hz, drive frequency 9.3 kHz, drive amplitude 244 mV, setpoint 311 mV. The CMAFM topograph was recorded in buffer solution at applied forces of ~100 pN.

details of the TMAFM topographs became more pronounced after correlation averaging and sixfold symmetrization (Fig. 1 *D*). The emanating arms connecting adjacent hexamers had a width of 5.9 ± 0.3 nm, the height difference to the V-shaped units was 1.7 ± 0.3 nm, and the maximum height of the protrusion was 1.9 ± 0.3 nm (Fig. 1 *D*). The symmetrized standard deviation map (Fig. 1 *E*) had maxima (0.95 ± 0.1 nm) between adjacent HPI cores, and the SD was found to be enhanced (0.78 ± 0.1 nm) at the V-shaped topographic protrusions and at the center of the hexameric core.

These TMAFM data were compared to the analogous set obtained by CMAFM (Fig. 1, *F* and *G*) (Müller et al., 1998). In the latter, the donut-shaped hexamers clearly featured six V-shaped protrusions and spokes that form the intermolecular links (Fig. 1 *F*). These emanating arms had a width of 4.5 ± 0.3 nm, the height difference to the V-shaped units was 2.2 nm ± 0.3 nm, and the maximum height of the protrusion was 2.7 ± 0.3 nm. The SD map exhibited maxima (0.34 nm) between the spokes (Fig. 1 *G*).

The TMAFM topographs exhibited a similar lateral resolution and a good correlation to structures obtained by CMAFM, but the heights were ~25% smaller than those from CMAFM. However, the SD map obtained from TMAFM topographs exhibited enhanced minimum and maximum values and showed a morphology quite different than that from CMAFM.

High-resolution tapping-mode topographs of purple membrane

Purple membrane consists of 75% (w/w) bacteriorhodopsin and 25% lipids (Kates et al., 1982). Bacteriorhodopsin oligomerizes into trimers that assemble into a 2-D trigonal lattice (a = 6.2 nm). Each subunit consists of seven transmembrane α-helices (Henderson et al., 1990) surrounding the photoreactive retinal (Jubb et al., 1984). The first atomic model of bacteriorhodopsin was derived from electron crystallography to a resolution of 0.35 nm (Henderson et al., 1990). Since then, five atomic models of bacteriorhodopsin have been solved by electron (Grigorieff et al., 1996; Kimura et al., 1997) and by x-ray crystallography (Pebay-Peyroula et al., 1997; Essen et al., 1998; Luecke et al., 1998).

TMAFM topographs of the extracellular purple membrane surface exhibited trimeric structures protruding 0.4 ± 0.1 nm (n = 161) above the lipid bilayer (Fig. 2 *A*). The trimers were arranged in a trigonal lattice of 6.2 ± 0.2 nm side length. However, the noise limited further details of the image to be recognized, and correlation averaging was required to enhance the signal-to-noise ratio (Fig. 2 *B*). After this, a major and a minor trimeric protrusion arranged on equilateral triangles could be distinguished. The major domains (height 0.4 nm) were separated by 2.8 nm, and the three minor domains (height 0.1 nm) were 1.7 nm apart. The

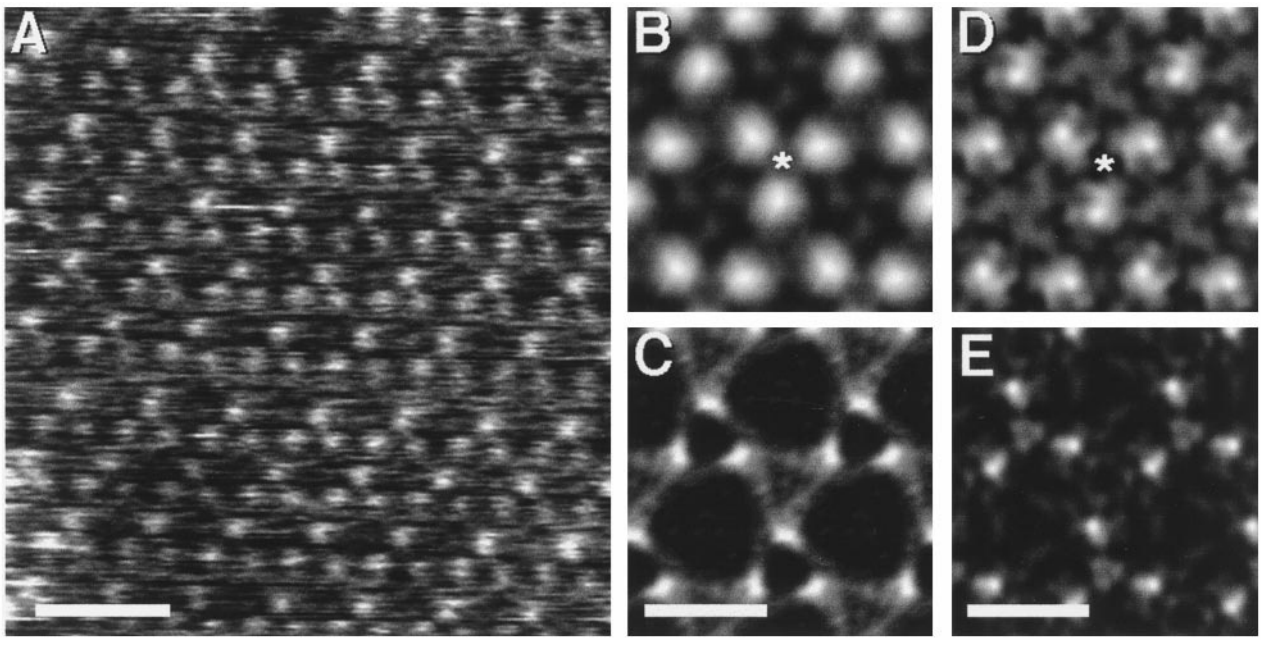

FIGURE 2 TMAFM topograph of the extracellular purple membrane surface. (*A*) Raw data obtained in 300 mM KCl, pH 7.8, 10 mM Tris-HCl. (*B*) Threefold symmetrized correlation average (n = 35; 16.3% RMS deviation from threefold symmetry). (*C*) Threefold symmetrized SD map. (*D*) Averaged topograph of the extracellular purple membrane surface, recorded by CMAFM. The correlation average was threefold symmetrized (n = 320; 6.1% RMS deviation from threefold symmetry; Müller et al., 1999b). (*E*) Threefold symmetrized standard deviation map of *D*. The asterisk marks the center of the bacteriorhodopsin trimer. Full gray-level ranges: 1.5 nm (*A*), 1 nm (*B* and *D*). Minima and maxima of the SD maps were 0.09 nm and 0.15 nm for *C* and 0.07 nm and 0.12 nm for *E*. Scale bars: 10 nm (*A*) and 5 nm (*C* and *E*). TMAFM imaging conditions: purple membrane adsorbed onto mica, original scan size 50 nm, scan frequency 5.8 Hz, drive frequency 8.8 kHz, drive amplitude 25 mV, setpoint 21 mV. The CMAFM topograph was recorded in buffer solution at applied forces of ~100 pN.

symmetrized SD exhibited minima (0.09 nm) over the minor domains, reflecting the relative stiffness of this structure (Fig. 2 *C*). Larger height fluctuations occurred at the outer edges of the major protrusions, resulting in a standard deviation of 0.15 nm.

Again, TMAFM and CMAFM topographs were compared to assess whether the former faithfully represented the structure of bacteriorhodopsin (Fig. 2, *D* and *E*) (Müller et al., 1999b). The extracellular surface consisted of tripartite protrusions arranged on a trigonal lattice (Fig. 2 *D*), with a maximum height difference between the protein and the lipid membrane of 0.5 ± 0.1 nm ($n = 320$). As reported previously (Müller et al., 1999b), the major protrusion of this surface represents the antiparallel β-strand connecting transmembrane α-helices B and C of bacteriorhodopsin. The elongated minor protrusion represents the loop connecting α-helices F and G of bacteriorhodopsin. The SD map had maxima (0.12 nm) at the rim of each major protrusion, where the flexible N-terminus of bacteriorhodopsin is located (Fig. 2 *E*).

Although TMAFM topographs of the extracellular purple membrane surface exhibited a lower resolution, they can be correlated to averages obtained from the contact-mode topographs (Fig. 2 *D*; Müller et al., 1999b). In agreement with the SD calculated from contact mode topographs (Fig. 2 *E*, *bottom*), the maximum of the SD map was located at the outer rim of the major topographic protrusion. However, the minimum and maximum of the SD map calculated from TMAFM topographs were ~25% higher.

Sensitivity of tapping-mode imaging

When imaged by TMAFM at minimal forces, the cytoplasmic purple membrane surface also revealed three peripheral protrusions (Fig. 3 *A*) that became distinct after correlation averaging of 307 unit cells (Fig. 3 *B*). As shown previously, the protrusions arise from the loop connecting transmembrane α-helices E and F (Müller et al., 1995a). Their intertrimeric distance in the symmetrized correlation-averaged topograph corresponds to ~3.5 nm, and their height above the lipid bilayer was 0.9 ± 0.2 nm ($n = 37$). The minimum SD of the averaged topograph was 0.22 nm, and the major protrusions exhibited a maximum SD of 0.33 nm (Fig. 3 *C*). This protrusion was not present in TMAFM topographs recorded at higher applied forces as previously observed by CMAFM. However, this deformed the bacteriorhodopsin surface by the interaction with the scanning stylus rather profoundly, hindering reproducible submolecular resolution of the shorter loops connecting transmembrane α-helices (data not shown) (Müller et al., 1995a).

In comparison, CMAFM topographs of the cytoplasmic purple membrane surface revealed bacteriorhodopsin trimers with three peripheral protrusions of 0.8 ± 0.1 nm height

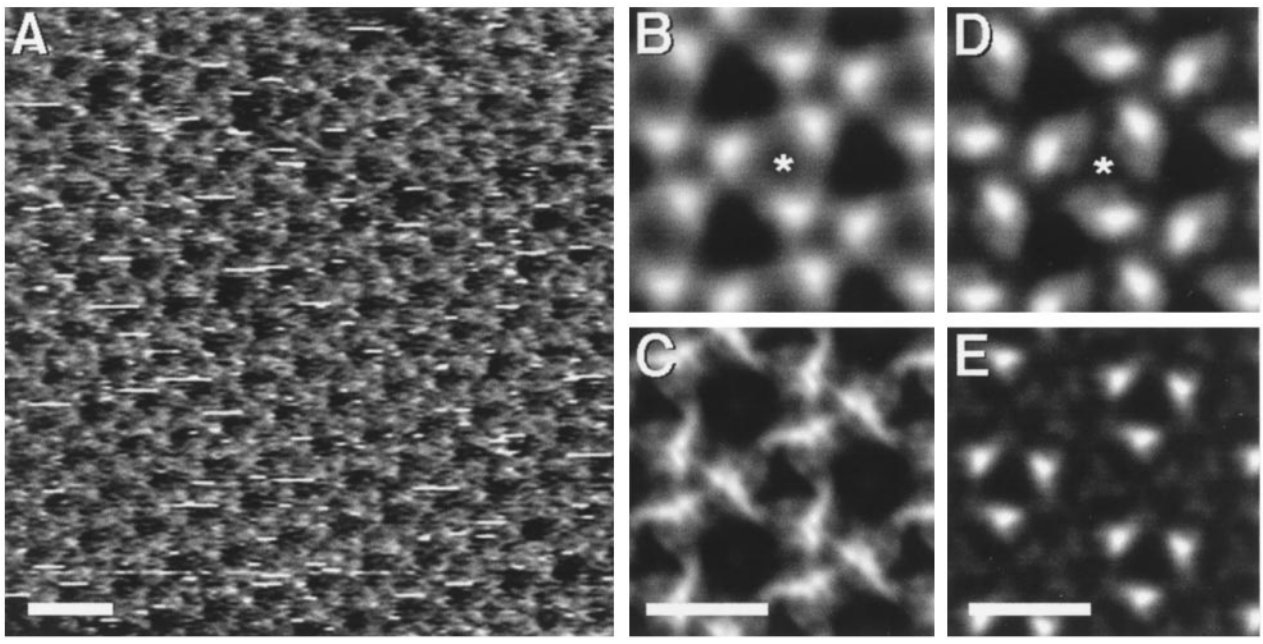

FIGURE 3 TMAFM topograph of the cytoplasmic purple membrane surface. (*A*) Raw data obtained in 100 mM KCl, pH 7.8, 10 mM Tris-HCl. (*B*) Threefold symmetrized correlation average ($n = 307$; 13% RMS deviation from threefold symmetry). (*C*) Threefold symmetrized SD map. (*D*) Averaged topograph of the cytoplasmic purple membrane surface recorded using CMAFM. The correlation average was threefold symmetrized (*top*; $n = 398$; 9.2% RMS deviation from threefold symmetry; Müller et al., 1999b). (*E*) Threefold symmetrized standard deviation map of *D*. The asterisk marks the center of the bacteriorhodopsin trimer. Full gray-level ranges: 1.5 nm (*A*), 1 nm (*B* and *D*). Minima and maxima of the SD maps were 0.22 nm and 0.33 nm for *C* and 0.08 nm and 0.17 nm for *E*. Scale bars: 10 nm (*A*) and 5 nm (*C* and *E*). TMAFM imaging conditions: purple membrane adsorbed onto mica, original scan size 180 nm, scan frequency 4 Hz, drive frequency 8.5 kHz, drive amplitude 95 mV, setpoint 11 mV. The CMAFM topograph was recorded in buffer solution at applied forces of ~100 pN.

(Fig. 3 *D*). Fig. 3 *E* displays the SD map, which showed pronounced maxima (0.19 nm) located at the positions of the topographic protrusions (Fig. 3 *D*), whereas the minima (0.1 nm) indicated the lipids.

Although the resolution of the TMAFM was lower, there was a good correlation to the surface structures obtained from CMAFM topographs. Interestingly, the two SD maps were similar, although that calculated from TMAFM topographs exhibited higher minimum and maximum values.

DISCUSSION

Our results demonstrate that resolution, S/N ratio, and sensitivity of tapping-mode atomic force microscopy are clearly sufficient to resolve submolecular details of proteins. The first topographs of the HPI layer recorded by TMAFM revealed little information beyond the 18 mm lattice (Schabert and Rabe, 1996). The averages calculated from the TMAFM topographs of HPI layer and purple membrane exhibited a lateral resolution between 1.1 and 1.5 nm, which is close to the range achievable with CMAFM (Table 1). Although the lateral resolution achieved with CMAFM on purple membrane is higher, there is a good structural correlation between the topographs recorded in the two imaging modes. However, comparison of SD values calculated from TMAFM and from CMAFM topographs shows that the minimum SD of TMAFM topographs was higher. The minimum of the SD represents to some extent the noise of the topograph resulting from the instrumental set-up. Interestingly, the differences between maximum and minimum SD are about the same in TMAFM and CMAFM (Table 1). In other words, the protein flexibility appears to be independent of the imaging mode used.

The TMAFM scanning parameters given in the Materials and Methods were found to be optimal for the purposes of this study. They strongly depend on the quality of the support, sample cleanliness, the adjustment of the microscope, and, most importantly, the type of cantilevers used. Changing the cantilever type often required a change of the drive frequency. To achieve high-resolution images, we had to individually adjust the tapping and scanning parameters (drive amplitude, drive frequency, gains, scan frequency, setpoint). Our conclusion is that high resolution can be achieved even if different cantilever types are used that possess different resonance frequencies and force constants. However, an important prerequisite is a good coupling between the fluid cell oscillations and the cantilever. Therefore, spectra of the cantilevers and cell should exhibit an overlapping region at the tapping frequency used (Schäffer et al., 1996).

Surprisingly, thermal drift had a major influence determining whether high-resolution TMAFM topographs could be achieved. The compensation for the thermal drift was adjusted manually by correcting the setpoints (see Materials and Methods). The correction of the setpoint had to be made in very small steps (0.001 V). In the near future, the setpoint will be automatically adjusted at the end of every scan line to compensate for drift in the *z* direction.

In contact mode, high-resolution topographs can be obtained by exploiting electrostatic interactions to balance the overall forces between the stylus and the fragile biological sample (Müller et al., 1999a). In this way, the force applied to the cantilever can be distributed over a larger area, and a small protrusion on the stylus can contour submolecular structures, using small deviations of the applied force for the feedback of the servo system. If the electrolyte is adjusted properly, friction, wear, and deformation are minimized, allowing reproducible subnanometer resolution of native proteins. We have attempted to determine whether the electrolyte has an influence on the resolution of TMAFM. Unexpectedly, the type of electrolyte and its concentration had no detectable influence on the quality of the topographs.

The sensitivity of the TMAFM imaging process was best demonstrated on the cytoplasmic surface of purple membrane, as we were able to image the most prominent polypeptide loop-connecting transmembrane α-helices E and F. The energy required to bend this loop is $\sim$12 kJ/mol, corresponding to an applied force of $>$100 pN (Müller et al., 1999b). This result is the strongest indication so far that TMAFM is capable of faithfully imaging individual peptide segments. However, it was not possible to image the shorter cytoplasmic loops on the bacteriorhodopsin molecule. At setpoints (amplitude damping) corresponding to forces that displace the EF loop, the oscillating stylus deformed the protein surface, making it impossible to image the smaller loops. Under such enhanced forces the interaction time between stylus and sample increases (Garcia et al., 1995). As a consequence, the harmonic oscillation of the cantilever required for high-resolution imaging might be significantly influenced, precluding proper tracking of the sample. We

TABLE 1 Comparing heights, standard deviations (SDs), and the resolution revealed by TMAFM and CMAFM

	TMAFM			CMAFM		
Sample	Height (nm)	SD (nm)	Resolution (nm)	Height (nm)	SD (nm)	Resolution (nm)
Outer HPI layer surface	1.7 ± 0.3*	0.62–0.95	~1.5	2.2 ± 0.3*	0.11–0.34	~1.5
Extracellular purple membrane surface	0.4 ± 0.1#	0.09–0.15	~1.1	0.5 ± 0.1#	0.07–0.12	≤0.5
Cytoplasmic purple membrane surface	0.6 ± 0.1#	0.22–0.33	~1.2	0.8 ± 0.1#	0.08–0.17	≤0.5

*Height difference measured from V-shaped protrusions to the emanating arms.

#Height difference of the maximum protrusion over the lipid bilayer.

The lateral resolution of all topographs was determined by the spectral signal-to-noise ratio (Unser et al. 1989) and by the spatial frequency correlation (Schabert and Engel, 1994). Resolutions presented in the table represent the lower values found by either one of both criteria.

found that this effect was best studied on soft biological samples with known surface structures. The topographs recorded under such conditions were inhomogenous and were not reproducible (data not shown). At even higher setpoints the protein surfaces were easily disrupted in an uncontrolled manner by the oscillating tip.

The standard deviation map of the HPI layer showed pronounced maxima in the open areas between the spokes that cannot be correlated with the protein structure (Baumeister et al., 1986). During tapping of the protein surface, the feedback loop of the TMAFM keeps the amplitude change constant. Thus, while over a hole, the stylus is pushed forward until its side interacts with the rim of the hole. In this case, the contact area between the stylus and sample is ill defined, explaining the pronounced standard deviation maxima at the gaps between adjacent cores of the HPI layer.

The six V-shaped protrusions at the periphery of the HPI core exhibited a lower standard deviation. Similarly, the SD map obtained from topographs recorded in contact mode showed some variability of these structures (Müller et al., 1998). Obviously, this variability was independent of the imaging process used. Although the two averages exhibit a similar resolution (~1.5 nm), the SD calculated from TMAFM topographs was more detailed than the one calculated from the CMAFM topographs and exhibited features similar to that of the V-shaped protrusions. The resolution of the SD map, lying close to 1 nm, allows a detailed assignment of their structural flexibilities.

CONCLUSIONS

Tapping-mode AFM allows imaging of native protein surfaces at submolecular resolution in buffer solution. A lateral resolution between 1.1 and 1.5 nm and a vertical resolution between 0.1 and 0.2 nm was achieved. The resolution achieved on the HPI layer was similar in TMAFM and CMAFM (~1.5 nm); in the case of purple membrane the resolution of TMAFM topographs (~1.1–1.2 nm) was less than the resolution achieved using CMAFM (≤0.5 nm). Although the standard deviation (SD) maps exhibited a higher minimum (between 0.1 and 0.9 nm), the difference between maxima and minima of the SD remained in a range similar to that observed for CMAFM topographs. TMAFM is sufficiently sensitive to image individual peptide loops connecting transmembrane α-helices in their native, extended conformation. Based on these results, it appears that new instrumentation that operates stably for even lower oscillation amplitudes (beneath 1 nm) and an automatically adjusted setpoint will produce even lower force measurements at higher spatial resolutions. Therefore, tapping mode might be used in the future to observe substructures of macromolecular systems that cannot be firmly immobilized. These include individual proteins or protein complexes, filamentous structures, and loosely attached extrinsic membrane protein complexes.

We thank Dr. Wolfgang Baumeister and Dr. Georg Büldt for the biological samples. DM thanks G. Büldt for his continuous encouragement and support. We thank Dr. Bernhard Heymann, Dr. Joerg Kistler, Dr. Shirley Müller, and Martin Stark for very valuable discussions and critical reading of the manuscript. We are grateful to the Max Planck Institute for Molecular Cell Biology and Genetics at Dresden for providing one of the TMAFMs used.

This work was supported by the Swiss National Foundation for Scientific Research (grant 31-42435.94) and the Maurice E. Müller Foundation of Switzerland.

REFERENCES

Amrein, M., Z. Wang, and R. Guckenberger. 1991. Comparative study of a regular protein layer by scanning tunneling microscopy and transmission electron microscopy. *J. Vac. Sci. Techol. B.* 9:1276–1281.

Baumeister, W., M. Barth, R. Hegerl, R. Guckenberger, M. Hahn, and W. O. Saxton. 1986. Three-dimensional structure of the regular surface layer (HPI layer) of *Deinococcus radiodurans. J. Mol. Biol.* 187: 241–253.

Baumeister, W., F. Karrenberg, R. Rachel, A. Engel, B. Ten Heggeler, and W. O. Saxton. 1982. The major cell envelope protein of *Micrococcus radiodurans* (R1). *Eur. J. Biochem.* 125:535–544.

Bezanilla, M., B. Drake, E. Nudler, M. Kashlev, P. K. Hansma, and H. G. Hansma. 1994. Motion and enzymatic degradation of DNA in the atomic force microscope. *Biophys. J.* 67:2454–2459.

Binnig, G., C. F. Quate, and C. Gerber. 1986. Atomic force microscope. *Phys. Rev. Lett.* 56:930–933.

Bremer, A., C. Henn, A. Engel, W. Baumeister, and U. Aebi. 1992. Has negative stain still a place in biomacromolecular electron microscopy? *Ultramicroscopy.* 46:85–111.

Butt, H.-J. 1992. Measuring local surface charge densities in electrolyte solutions with a scanning force microscope. *Biophys. J.* 63:578–582.

Butt, H.-J., and M. Jaschke. 1995. Calculation of thermal noise in atomic force microscopy. *Nanotechnology.* 6:1–7.

Colton, R., A. Engel, J. Frommer, H. Gaub, G. Gewirth, R. Guckenberger, W. Heckl, B. Parkinson, and J. Rabe, editors. 1998. Procedures in Scanning Probe Microscopy. John Wiley and Sons, Chichester.

Czajkowsky, D., M. Allen, V. Elings, and Z. Shao. 1998a. Direct visualization of surface charge in aqueous solution. *Ultramicroscopy.* 74:1–5.

Czajkowsky, D. M., S. Sheng, and Z. Shao. 1998b. Staphylococcal α-hemolysin can form hexamers in phospholipid bilayers. *J. Mol. Biol.* 276:325–330.

Drake, B., C. B. Prater, A. L. Weisenhorn, S. A. C. Gould, T. R. Albrecht, C. F. Quate, D. S. Cannell, H. G. Hansma, and P. K. Hansma. 1989. Imaging crystals, polymers, and processes in water with the atomic force microscope. *Science.* 243:1586–1588.

Dunlap, D. D., A. Maggi, M. R. Soria, and L. Monaco. 1997. Nanoscopic structure of DNA condensed for gene delivery. *Nucleic Acids Res.* 25:3095.

Engel, A., W. Baumeister, and W. Saxton. 1982. Mass mapping of a protein complex with the scanning transmission electron microscope. *Proc. Natl. Acad. Sci. USA.* 79:4050–4054.

Engel, A., Y. Lyubchenko, and D. J. Müller. 1999. Atomic force microscopy: a powerful tool to observe biomolecules at work. *Trends Cell Biol.* 9:77–80.

Essen, L.-O., R. Siegert, W. D. Lehmann, and D. Oesterhelt. 1998. Lipid patches in membrane protein oligomers: crystal structure of the bacteriorhodopsin-lipid complex. *Proc. Natl. Acad. Sci. USA.* 95: 11673–11678.

Fritz, M., M. Radmacher, M. W. Allersma, J. P. Cleveland, R. J. Stewart, P. K. Hansma, and C. F. Schmidt. 1995a. Imaging microtubules in buffer solution using tapping mode atomic force microscopy. *SPIE.* 2384: 150–157.

Fritz, M., M. Radmacher, J. P. Cleveland, M. W. Allersma, R. J. Steward, R. Gieselmann, P. Janmey, C. F. Schmidt, and P. K. Hansma. 1995b. Imaging globular and filamentous proteins in physiological buffer solutions with tapping mode atomic force microscopy. *Langmuir.* 11: 3529–3535.

Garcia, R., J. Tamayo, J. M. Soler, and C. Bustamate. 1995. Physical parameters that control the imaging of purple membrane with the scanning tunneling microscope. *Langmuir.* 11:2109–2114.

Grigorieff, N., T. A. Ceska, K. H. Downing, J. M. Baldwin, and R. Henderson. 1996. Electron-crystallographic refinement of the structure of bacteriorhodopsin. *J. Mol. Biol.* 259:393–421.

Guckenberger, R., W. Wiegräbe, A. Hillebrand, T. Hartman, Z. Wang, and W. Baumeister. 1989. Scanning tunneling microscopy of a hydrated bacterial surface protein. *Ultramicroscopy.* 31:327–332.

Hansma, P. K., J. P. Cleveland, M. Radmacher, D. A. Walters, P. E. Hillner, M. Bezanilla, M. Fritz, D. Vie, H. G. Hansma, C. B. Prater, J. Massie, L. Fukunaga, J. Gurley, and V. Elings. 1994. Tapping mode atomic force microscopy in liquids. *Appl. Phys. Lett.* 64:1738–1740.

Henderson, R., J. M. Baldwin, T. A. Ceska, F. Zemlin, E. Beckman, and K. H. Downing. 1990. Model for the structure of bacteriorhodopsin based on high-resolution electron cryo-microscopy. *J. Mol. Biol.* 213: 899–929.

Hoh, J. H., G. E. Sosinsky, J.-P. Revel, and P. K. Hansma. 1993. Structure of the extracellular surface of the gap junction by atomic force microscopy. *Biophys. J.* 65:149–163.

Hörber, J. K. H., H. Fuchs, R. J. Behm, and R. Wiesendanger, editors. 1998. Scanning tunneling microscopy/spectroscopy and related techniques. *Appl. Phys.* A 66.

Jakubowski, U., R. Hegerl, H. Formanek, S. Volker, U. Santarius, and W. Baumeister. 1988. Three-dimensional reconstruction of the HPI-layer of *Deinococcus radiodurans* embedded in Cd-thioglycerol. *In* 9th European Congress on Electron Microscopy York, England. H. G. Dickinson and P. J. Goodhews. Institute of Physics, Bristol, England. 381–382.

Jubb, J. S., D. L. Worcester, H. L. Crespi, and G. Zaccai. 1984. Retinal location in purple membrane of *Halobacterium halobium*: a neutron diffraction study of membranes labeled in vivo with deuterated retinal. *EMBO J.* 3:1455–1461.

Karrasch, S., M. Dolder, J. Hoh, F. Schabert, J. Ramsden, and A. Engel. 1993. Covalent binding of biological samples to solid supports for scanning probe microscopy in buffer solution. *Biophys. J.* 65: 2437–2446.

Karrasch, S., R. Hegerl, J. Hoh, W. Baumeister, and A. Engel. 1994. Atomic force microscopy produces faithful high-resolution images of protein surfaces in an aqueous environment. *Proc. Natl. Acad. Sci. USA.* 91:836–838.

Kasas, S., N. H. Thomson, B. L. Smith, H. G. Hansma, X. Zhu, M. Guthold, C. Bustamante, E. T. Kool, M. Kashlev, and P. K. Hansma. 1997. *Escherichia coli* RNA ploymerase activity observed using atomic force microscopy. *Biochemistry.* 36:461–468.

Kates, M., S. C. Kushawa, and G. D. Sprott. 1982. Lipids of purple membrane from extreme halophiles and of methanogenic bacteria. *Methods Enzymol.* 88:98–111.

Kimura, Y., D. G. Vassylev, A. Miyazawa, A. Kidera, M. Matsushima, K. Mitsuoka, K. Murata, T. Hirai, and Y. Fujiyoshi. 1997. Surface of bacteriorhodopsin revealed by high-resolution electron microscopy. *Nature.* 389:206–211.

Luecke, H., H.-T. Richter, and J. K. Lanyi. 1998. Proton transfer pathways in bacteriorhodopsin at 2.3 Angstrom resolution. *Science.* 280: 1934–1937.

Lyubchenko, Y. L., and L. S. Shlyakhtenko. 1997. Direct visualization of supercoiled DNA in situ with atomic force microscopy. *Proc. Natl. Acad. Sci. USA.* 94:496–501.

Martin, L. D., J. P. Vesenka, E. Henderson, and D. L. Dobbs. 1995. Visualization of nucleosomal substructure in native chromatin by atomic force microscopy. *Biochemistry.* 34:4610–4616.

Müller, D. J., M. Amrein, and A. Engel. 1997a. Adsorption of biological molecules to a solid support for scanning probe microscopy. *J. Struct. Biol.* 119:172–188.

Müller, D. J., W. Baumeister, and A. Engel. 1996a. Conformational change of the hexagonally packed intermediate layer of *Deinococcus radiodurans* imaged by atomic force microscopy. *J. Bacteriol.* 178: 3025–3030.

Müller, D. J., G. Büldt, and A. Engel. 1995a. Force-induced conformational change of bacteriorhodopsin. *J. Mol. Biol.* 249:239–243.

Müller, D. J., and A. Engel. 1997. The height of biomolecules measured with the atomic force microscope depends on electrostatic interactions. *Biophys. J.* 73:1633–1644.

Müller, D. J., and A. Engel. 1999. pH and voltage induced structural changes of porin OmpF explain channel closure. *J. Mol. Biol.* 285: 1347–1351.

Müller, D. J., D. Fotiadis, and A. Engel. 1998. Mapping flexible protein domains at subnanometer resolution with the AFM. *FEBS Lett.* 430: 105–111.

Müller, D. J., D. Fotiadis, S. Scheuring, S. A. Müller, and A. Engel. 1999a. Electrostatically balanced subnanometer imaging of biological specimens by atomic force microscopy. *Biophys. J.* 76:1101–1111.

Müller, D. J., H.-J. Sass, S. Müller, G. Büldt, and A. Engel. 1999b. Surface structures of native bacteriorhodopsin depend on the molecular packing arrangement in the membrane. *J. Mol. Biol.* 285:1903–1909.

Müller, D. J., F. A. Schabert, G. Büldt, and A. Engel. 1995b. Imaging purple membranes in aqueous solutions at subnanometer resolution by atomic force microscopy. *Biophys. J.* 68:1681–1686.

Müller, D. J., C. A. Schoenenberger, G. Büldt, and A. Engel. 1996b. Immuno-atomic force microscopy of purple membrane. *Biophys. J.* 70:1796–1802.

Müller, D. J., C.-A. Schoenenberger, F. Schabert, and A. Engel. 1997b. Structural changes of native membrane proteins monitored at subnanometer resolution with the atomic force microscope. *J. Struct. Biol.* 119: 149–157.

Oesterhelt, D. 1998. The structure and mechanism of the family of retinal proteins from halophilic archaea. *Curr. Opin. Struct. Biol.* 8:489–500.

Oesterhelt, D., and W. Stoeckenius. 1973. Functions of a new photoreceptor membrane. *Proc. Natl. Acad. Sci. USA.* 70:2853–2857.

Oesterhelt, D., and W. Stoeckenius. 1974. Isolation of the cell membrane of *Halobacterium halobium* and its fraction into red and purple membrane. *Methods Enzymol.* 31:667–678.

Pebay-Peyroula, E., G. Rummel, J. P. Rosenbusch, and E. M. Landau. 1997. X-ray structure of bacteriorhodopsin at 2.5 angstroms from microcrystals grown in lipidic cubic phases. *Science.* 277:1676–1681.

Peters, J., M. Peters, F. Lottspeich, W. Schäfer, and W. Baumeister. 1987. Nucleotide sequence of the gene encoding the *Deinococcus radiodurans* surface protein, derived amino acid sequence, and complementary protein chemical studies. *J. Bacteriol.* 169:5216–5223.

Putman, C. A. J., K. van der Werft, B. G. de Grooth, N. F. van Hulst, J. Greve, and P. K. Hansma. 1992. A new imaging mode in the atomic force microscopy based on the error signal. *SPIE.* 1639:198–204.

Putman, C. A. J., K. O. Vanderwerf, B. G. Degrooth, N. F. Vanhulst, and J. Greve. 1994. Tapping mode atomic force microscopy in liquid. *Appl. Phys. Lett.* 64:2454–2456.

Radmacher, M., J. P. Cleveland, M. Fritz, H. G. Hansma, and P. K. Hansma. 1994a. Mapping interaction forces with the atomic force microscope. *Biophys J.* 66:2159–2165.

Radmacher, M., M. Fritz, H. G. Hansma, and P. K. Hansma. 1994b. Direct observation of enzyme activity with the atomic force microscopy. *Science.* 265:1577–1579.

Salapaka, M. V., H. S. Bergh, J. Lai, A. Majumdar, and E. McFarland. 1997. Multi-mode noise analysis of cantilevers for scanning probe microscopy. *J. Appl. Phys.* 81:2480–2487.

Saxton, W. O., and W. Baumeister. 1982. The corelation averaging of a regularly arranged bacterial cell envelope protein. *J. Microsc.* 127: 127–138.

Saxton, W. O., T. J. Pitt, and M. Horner. 1979. Digital image processing: the semper system. *Ultramicroscopy.* 4:343–354.

Schabert, F. A., and A. Engel. 1994. Reproducible acquisition of *Escherichia coli* porin surface topographs by atomic force microscopy. *Biophys. J.* 67:2394–2403.

Schabert, F. A., C. Henn, and A. Engel. 1995. Native *Escherichia coli* OmpF porin surfaces probed by atomic force microscopy. *Science.* 268:92–94.

Schabert, F. A., and J. P. Rabe. 1996. Vertical dimension of hydrated biological samples in tapping mode scanning force microscopy. *Biophys. J.* 70:1514–1520.

Schäffer, T. E., J. P. Cleveland, F. Ohnesorge, D. A. Walters, and P. K. Hansma. 1996. Studies of vibrating atomic force microscope cantilevers in liquid. *J. Appl. Phys.* 80:3622–3627.

Scheuring, S., D. J. Müller, P. Ringler, J. B. Heymann, and A. Engel. 1999. Imaging streptavidin 2D crystals on biotinylated lipid monolayers at high resolution with the atomic force microscopy. *J. Microsc.* 193: 28–35.

Shlyakhtenko, L. S., V. N. Potaman, R. R. Sinden, and Y. L. Lyubchenko. 1998. Structure and dynamics of supercoil-stabilized DNA cruciforms. *J. Mol. Biol.* 280:61–72.

Stemmer, A., R. Reichelt, R. Wyss, and A. Engel. 1991. Biological structures imaged in a hybrid scanning transmission electron microscope and scanning tunneling microscope. *Ultramicroscopy.* 35:255–264.

Unser, M., B. L. Trus, J. Frank, and A. L. Steven. 1989. The spectral signal-to-noise ration resolution criterion: computational efficiency and statistical precision. *Ultramicroscopy.* 30:429–434.

Wagner, P. 1998. Immobilization strategies for biological scanning probe microscopy. *FEBS Lett.* 430:112–115.

Wang, Z., T. Hartman, W. Baumeister, and R. Guckenberger. 1990. Thickness determination of biological samples with a z-calibrated scanning tunneling microscope. *Proc. Natl. Acad. Sci. USA.* 87:9343–9347.

Wiesendanger, R. 1994. Scanning Probe Microscopy and Spectroscopy: Methods and Applications. Cambridge University Press, Cambridge.

Yang, J., J. X. Mou, and Z. F. Shao. 1994. Molecular resolution atomic force microscopy of soluble proteins in solution. *Biochim. Biophys. Acta.* 1199:105–114.

Yang, J., L. K. Tamm, T. W. Tillack, and Z. Shao. 1993. New approach for atomic force microscopy of membrane proteins. *J. Mol. Biol.* 229: 286–290.

Zhong, Q., D. Inniss, K. Kjoller, and V. B. Elings. 1993. Fractured polymer/silica fiber surface studied by tapping mode atomic force microscopy. *Surf. Sci. Lett.* 290:L688–L692.